Science and Technology for Energy Transition **77**, 21 (2022)

https://doi.org/10.2516/stet/2022020

Available online at:
stet-review.org

REGULAR ARTICLE OPEN ACCESS

Smart detection of fractures in formation image logs for enhanced CO_2 storage

Klemens Katterbauer[1,*], Abdulaziz Al Qasim[1], Abdallah Al Shehri[1], and Rabeah Al Zaidy[2]

[1] Saudi Aramco, Dhahran, Saudi Arabia
[2] KFUPM, Dhahran, Saudi Arabia

Received: 13 February 2022 / Accepted: 10 October 2022

Abstract. Carbon capture and storage (CCS) has attracted strong interest from industry and the scientific community alike due to the ability of storing CO_2 in subsurface reservoirs. Deep saline aquifers may be well suited for the safe and long-term storage given their geological structure. The long term underground storage in saline aquifers depends on variety of interrelated trapping mechanisms in addition to the caprock sealing efficiency. Fractures are commonplace in many geological settings and represent a crucial role for hydrocarbon migrations and entrapment. Fracture impact fluid flow in variety of forms, particularly due to the complexity and varying natures of the fractures, which channel the injected CO_2 throughout the reservoir formation. This is especially important for tight gas reservoirs and low permeable cap rock structures whose permeability is primarily characterized by the fault and fractures. This outlines the importance of determining accurately fracture penetration in wellbores for CO_2 injection. We present a new deep learning framework for the detection of fractures in formation image logs for enhancing CO_2 storage. Fractures may represent high velocity gas flow channels which may make CO_2 storage a challenge. The novel deep learning framework incorporates both acoustic and electrical formation image logs for the detection of fractures in wellbores for CO_2 storage enhancement and injection optimization. The framework was evaluated on the Pohokura-1 well for the detection of fractures, with the framework exhibiting strong classification accuracy. The framework could accurately classify the fractures based on acoustic and electrical image logs in 98.1% for the training and 85.6% for the testing dataset. Furthermore, estimates of the fracture size are strong, indicating the ability of the framework to accurately quantify fracture sizes in order to optimize CO_2 injection and storage.

Keywords: Formation image logs, CO_2 sequestration, Artificial intelligence, Image recognition, Sustainability.

1 Introduction

Carbon capture and storage (CCS) has attracted strong interest from industry and the scientific community alike due to the ability of storing CO_2 in subsurface reservoirs. Deep saline aquifers may be well suited for the safe and long-term storage given their geological structure. The long term underground storage in saline aquifers depends on variety of interrelated trapping mechanisms in addition to the caprock sealing efficiency. Furthermore, well integrity plays another critical role to reduce uncertainty. When evaluating CO_2 storage sites, both natural and artificially-induced hydraulic fractures are important factors to be taken into account for the risk assessment of the CO_2 storage (Ghiat and Al-Ansari, 2021). Fractures are commonplace in many geological settings and represent a crucial role for hydrocarbon migrations and entrapment. Fracture impact fluid flow in variety of forms, particularly due to the complexity and varying natures of the fractures, which channel the injected CO_2 throughout the reservoir formation. This is especially important for tight gas reservoirs and low permeable cap rock structures whose permeability is primarily characterized by the fault and fractures. For these fractures the spatial distribution of the faults and fractures, the orientation, conductivity and the overall contribution to the effective permeability are most essential to know. Furthermore it is critical to determine fractures interfacing with the wellbore given that they are the main channel for the CO_2 to flow into the reservoir (Tursunov *et al.*, 2017).

Determining the fracture penetration and structure is critical due to the fact that these fractures may pose potential escape patterns for the CO_2 that may impact the quality of the storage site. Generally, fractures have low storage

* Corresponding author: klemens.katterbauer@aramco.com

and high permeability values as compared to the surrounding matrix rock. The fractures may allow the CO_2 to migrate quickly to the cap rock, which may potentially also exhibit fractures. This would allow the CO_2 to move through the cap rock to the surface or into any adjacent aquifers (Andreasen, 2021).

Furthermore, the local pressure increases from CO_2 injection may also cause hydro-fracturing in the vicinity of the wells which may adapt the injection performance into the reservoir.

In order to characterize fracture structures and penetration, there are several different aspects to study. Seismic mapping has shown to be able to delineate well the overall reservoir structure, but challenges persist in mapping exact fracture channels given the limited resolution. Furthermore, the limited resolution for fractures close to the wellbores makes seismic data alone not sufficiently accurate to resolve these fractures. Another key source for fracture interpretation are core samples. Core samples allow to identify fractures based on core images and core analysis data. While these data may provide crucial insight about the rock formation and structure, they may less provide accurate information about the fracture penetration in the wellbores (Wang *et al.*, 2020).

Formation image logs have been a major source of fracture interpretation in wells, providing an image of the fractures in the wellbore. The two major forms of formation image logs are those based on electrical and acoustic image logging. Electrical image logs determine fractures based on the conductivity contrasts between the fracture and the adjacent borehole wall (Aghli *et al.*, 2020). By contrast, acoustic image logs utilize ultrasonics in order to determine from the roughness or reflectivity of the borehole wall the fractures in the wellbore.

Electrical images are produced via the placement of pads together with arrays of electrodes against the borehole (Fornero *et al.*, 2019). The electrical potential is maintained during the placement. The data from multiple electrodes are then combined in order to produce the electrical conductivity images. As the current is passed into the borehole wall, electrical image logs measure the properties of the volume of rock within a few inches around the borehole wall. The number of electrodes, arrangement and pad dimension in addition to the borehole diameter determine the azimuthal coverage of the image with resolutions being close to 2 mm (Hassall *et al.*, 2004).

The acoustic image logs use transducers that emit and record the acoustic pulse. The pulse's travel time from the transducer against the wellbore formation and back, which enables to deduce the dimension of the borehole and relative position. The returning amplitude, which is the energy of the returning pulse, incorporates the degree of scattering and the acoustic impedance contrast between borehole fluid and wall. Acoustic impedance and scattering depends on the borehole shape and rugosity as well as contrast between the different phases (Vidal *et al.*, 2016).

In order to interpret the data, planar fractures are shown as sine waves in the images. If fractures have large apparent aperture and they exhibit a distinction between the neighboring fractures, then these fractures can be relatively easily determined with both electrical and acoustic image logs. If the fractures are slightly non-planar or the areas exhibiting high fracture density, then determining these with electrical image logs is challenging. Furthermore, crosscutting and abutting relations are harder to distinguish in electrical image logs as compared to acoustic image logs. In contrast, large faults visible in the electrical image logs or widening of the borehole indicated by a caliper log are typically harder to detect in acoustic image logs. This is due to the data loss caused by scattering of the signal along the rough borehole walls (Rezig, 2019).

These specifics outline the challenges that are faced by the interpretation of formation image logs and the complementary nature of acoustic and electrical image logs.

Artificial intelligence for image recognition has undergone a major transformation within the last several years becoming part of everyday life. Image recognition is the task of identifying objects within an image and determines the category to which it belongs. Image recognition mimics the process of how humans identify different objects and associate them with individual definitions. While many individuals associate image recognition with the recognition of faces or objects, similar technologies can be utilized for the detection of fractures in image logs. Image detection and image recognition may be sometimes used interchangeably but are technically different. Image detection focuses on the task of taking an image as input and determines various objects within it. For example, face detection is a specific feature in order to determine what objects are within an image and the sole objective is to distinguish one object from another as well as quantify the number of different pictures. Image recognition differs from image detection in that the objective is to identify the objects and recognize the category to which they belong. This can be done based on the whole image or a subsection of the image (Li *et al.*, 2018).

Image recognition can be addressed with several available machine learning techniques such as support vector machines, bag of features models, and the Viola-Jones algorithm. While machine learning models have enabled to perform strong statistical analysis and classify images, the classification accuracy has been limited with respect to complex image recognition tasks. Deep learning image recognition models, incorporating convolutional neural networks have provided better results for the detection of features in images even if the images are warped, stretched or altered (Valentín *et al.*, 2019).

Automatically detecting fractures in formation image logs has remained a considerable challenge nevertheless.

2 Literature review

Utilizing artificial intelligence for the detection and determination of fractures has been outlined by several researchers. El Ouahed *et al.* presented a neural network approach to estimate the fracture intensity and network map. These early results demonstrated the ability to characterize reservoirs early in terms of their fracture distribution El Ouahed *et al.* (2005). Tian and Daigle presented a machine learning

framework for the identification of fractures in scanning electron microscope (SEM) images from carbonate-rich shale and siliceous shale samples. The framework utilizes the tensor flow object-detection API to detect objects in images, and utilizes single-shot detector in combination with a mobile net model (Tian and Daigle, 2018). While the results are promising for the detection of fractures in SEM images, the same technique may not easily be applied to formation image logs. The fractures are fairly well resolved via extensive contrasts in the SEM images. This is different from formation image logs where the fractures are exhibited as features in the images, but do not outline a strong contrast. Bihani *et al.* presented a framework for the identification and segmentation of pores and grains in mudrocks based on SEM images. The framework integrates Google's DeepLab v3 architecture in order to overcome the challenges related to imaging artifacts and pixel grayscales (Bihani *et al.*, 2022). While the approach is promising, the framework applies mainly to the segmentation of images into pores and non-pores that are clearly characterized by image contrasts.

3 Methodology

We developed a new deep learning framework for the classification and fracture degree identification for formation image logs (Fig. 1). The deep learning framework integrates both electrical and ultrasonic image log segments and classifies the sections in terms of whether it contains fractures or not, as well as determines the degree of fractures. The framework consists of multi-dual layer deep learning framework that integrates both a classification and regression layer. The classification layer determines whether the section represented by the formation image logs contain fractures or not. The regression layer then determines the fracture degree, which is a percentage value of the extent of fractures within the considered area. The deep learning framework may integrate either ultrasonic image logs, or electrical image logs separately, or combine them for the identification. The layers consist of multiple fully Connected Layers that are connected to batch normalization layers, and a ReLU activation function. Furthermore, the framework then estimates both with a final classification layer the existence of fractures, and with a regression layer the degree of the fracture. The novelty of the framework is the integration of the classification layer into the regression estimates of the degree of fracture. Furthermore, the framework has an adaptive weighting scheme that optimizes the input image weights based on the image feature variations. Specifically, both vertical and horizontal image feature variations are computed, and subsequently normalized. Highly varying images, relative to the average, are attributed a lower weight as compared to those whose variation is less.

4 Results

The Pohokura gas field is located in the north–east of New Plymouth in the Taranaki Basin that is close to the

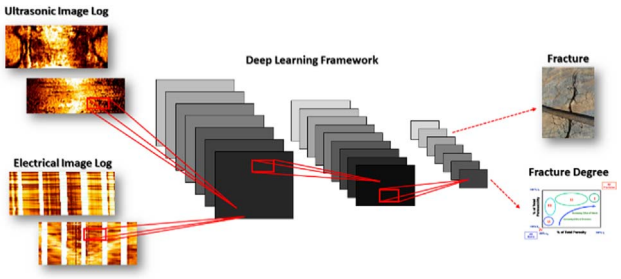

Figure 1. Deep learning framework for the fracture classification and fracture degree.

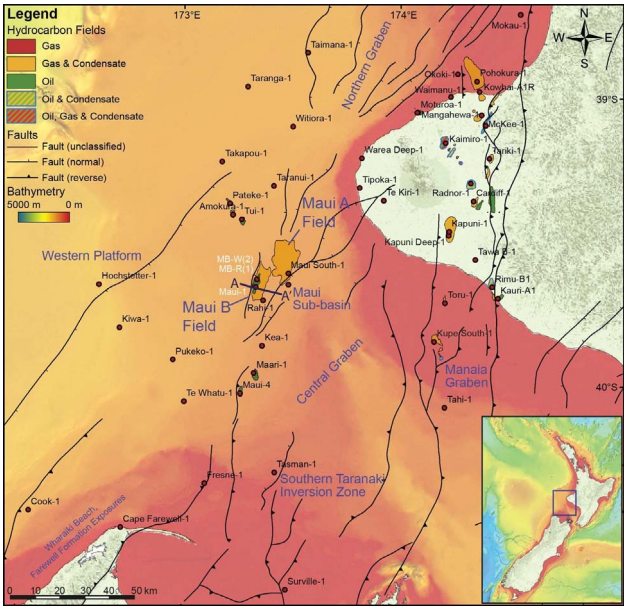

Figure 2. Map of central and southern Taranaki Basin with the Maui and Pohokura Fields indicated in orange.

Methanex Motunui site in Waitara (Fig. 2). The Taranaki Basin covers more than 100,000 km^2, primarily beneath the self and the continental slop that is offshore or in central-western of the North Island in New Zealand. The land sections are beneath the Taranaki Peninsula and in the northwest of the South Island. The basin incorporates a late Cretaceous to Quaternary sedimentary fill up that may be up to 8 km thick. This arose from the basin comprises an undeformed block and a heavily deformed area. The heavily deformed area contains the Taranaki Fault that leads to a Miocene basement overthrusting into the basin. The sedimentary fill of the Taranaki Basin may have arisen due to an intracontinental manifestation of a transform fault offsetting or a failed-rift (Three-Dimensional Structural and Petrophysical Modeling for Reservoir Characterization of the Mangahewa Formation, Pohokura Gas-Condensate Field, Taranaki Basin, New Zealand). There were several tectonic episodes that influenced the generation of the Taranaki Basin, which included the rifting between the cretaceous – Eocene period, the compression within the Eocene period and an extension

that arose from the late Miocene. The Pohokura files is the largest gas-condensate field and is a low-relief N–S trending anticline in the Northern Graben. The boundaries of the field are supported by the Taranaki Fault Zone in the east and the Cape Egmont Fault Zone in the west. The reservoir underwent compressional and extensional stress regimes and most of the drilling was in the northern part of the Pohokura Field. The petroleum play is a transgressive marginal marine sand within an inverted anticline. The coal seams of the Rakopi Formation are the main sources for the hydrocarbons in the Pohokura Field. The Rakopi Formation represents the deepest stratigraphic unit within the Taranaki Basin, and represents the major source for oil and gas fields within the basin. The Rakopi Formation is heavily dominated by fluvial-to-marginal marine lithofacies. The Mangahewa Formation from the Eocene Epoch is the primary reservoir zone, being the most prolific and thickest. The Mangahewa Formation contains interbedded sandstone, siltstone, mudstone and coal. The Turi Formation represents a top seal for the Pohokura Field and arose from Paleocene to the Eocene. The top seal is composed of non-calcareous, dark colored, micaceous and carbonaceous marine mudstone that is distributed throughout the Taranaki Basin.

The water depth is around 35 m in the block PMP 38154. The Taranaki Basin has several reservoirs that range from the Paleocene to Pliocene and is a gas-condensate field in a low-relief anticline, that is north-south elongated. The reservoir is 16 km long, and 5 km wide.

The Pohokura-1 well (Fig. 3) targeted the Kapuni group Mangahewa Formation sands in the Pohokura structure, where in total 700 m of shallow marine sands were encountered. The overall gas column extended to 130 m in the upper part of the Mangahewa structure. A deepening of the well was performed in order to potentially access the lower Mangahewa formation and reach the TD in the Mid-Eocene shales of the Omata formation. The lower part of the formation was not economically viable, and never produced gas condensates.

In order to measure the gas production performance, two drill stem tests were conducted in the upper section within the interval of 3625–3634 m MD and between 3553 and 3570 m MD. The flow measurements for the first interval were 3.5 MMSCF/D, and 16.5 MMSCF/D for the second interval. The well was rather valuable in mapping the reservoir with seismic data and has a control point for determining the overall structure of the Pohokura Field.

Based on existing well information from Pohokura 1, both adapted acoustic and electromagnetic image logs were obtained. The formation images were adapted within the interval of 3400–4200 m, which is the primary gas reservoir zone. These adapted formation image logs were manually classified in terms of whether they contained any fractures and how large these fractures are. For the manual classification both formation image logs, and other available well logs, such as borehole size, gamma ray, etc. were utilized. This manual classification was assumed to be the expert interpretation and ground truth for the determination of fracture and fracture extent. All the formation image logs were equalized in order to enhance interpretation.

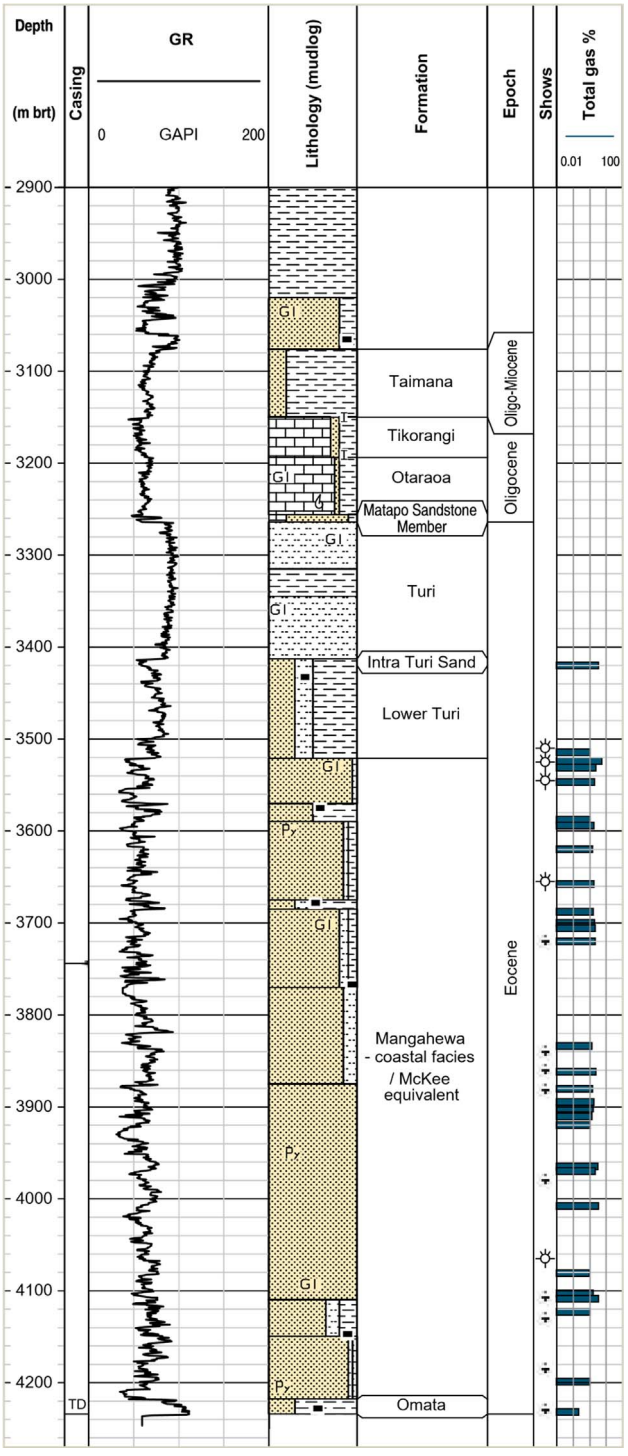

Figure 3. Pohokura-1 gas well.

The formation image logs were then vertically split into subimages, where a vertical resolution of 8 cm was used. These subimages were then classified in terms of whether they contained fractures or not, and also the degree of fracture was calculated for these images. The images were then integrated into an image datastore and labeled as well as its fracture degree was allocated. The overall fracture

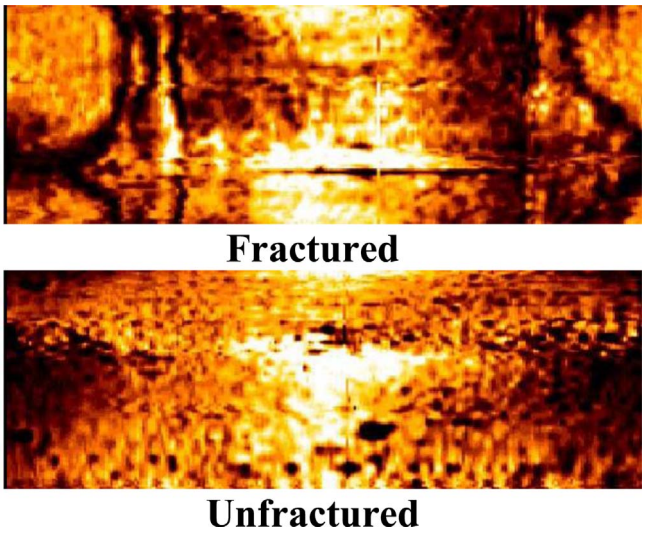

Figure 4. Formation acoustic image log images.

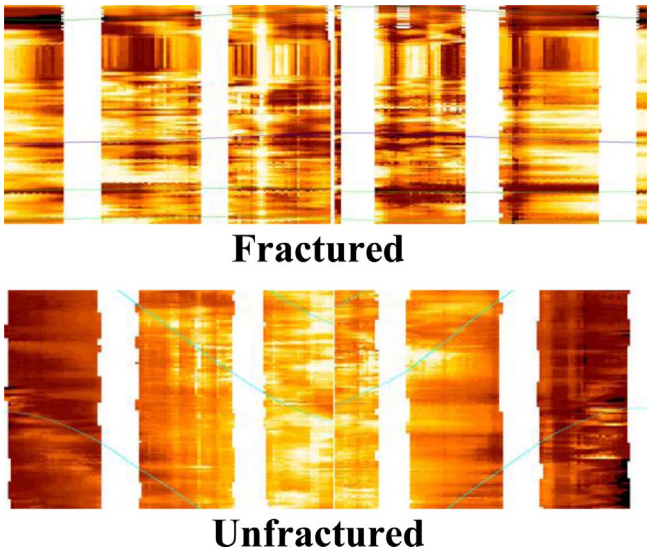

Figure 5. Formation electrical image log images.

distribution of the image datastore was 78.2% being composed of images with no fractures, and the remainder having various degrees of fractures. We present in Figures 4 and 5 sample acoustic and electrical image log images for the fracture detection image framework. The images exhibit fracture induced characteristics that based on expert interpretation and correlation with well logs and formation information allows to deduce the fractures and fracture size. However, the images themselves contain specific features such as fracture induced image contrasts that can be exploited by the deep learning framework.

We separated the image dataset into a training and testing dataset, utilizing an 80/20 split. Both datasets were ensured to be evenly distributed between fractured and unfractured images. Ensuring an even distribution is quintessential in order to avoid incorporating biases into the deep learning framework which may lead to overfitting and poor fracture identification. Furthermore, the framework does not take into account the depth at which the images were extracted. Depth independence is essential in order to allow the system to operate more general, and solely benefit from the features encountered in the images in order to detect fractures.

We present in Table 1 the performance of the fracture identification estimates. The results indicate strong performance when combining acoustic and electrical image logs and correctly classifying the images in terms of whether they contain fractures or not. While acoustic and electrical formation image logs by themselves may deliver acceptable results on the training set, the performance is less on the testing set. The results indicate strong estimation performance of the framework in detecting the fractures for optimizing CO_2 injection for CO_2 storage.

Determining the features that allow the deep learning image framework to distinguish images outlining fractures and those without fractures, we analyzed in greater detail which pixel parts have the most significant impact on the classification results. Figure 6 outlines some of the sub-images being strongly weighted for the determination of

Table 1. Deep learning performance of the fracture image framework.

	Training (%)	Testing (%)
Acoustic alone	81.5	62.4
Electrical alone	82.5	60.1
Combined	98.1	85.6

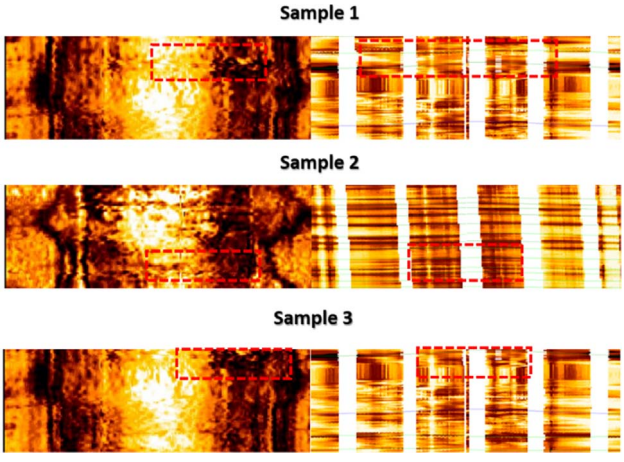

Figure 6. Features in images indicating the presence of fractures.

the presence of fractures in the imaging framework. Specifically, the contrast between the sections of intensity in both the acoustic and electrical image logs is well observed that are indicative of disconformities in the wellbore area.

In a final step, the framework quantifies the fracture size based on the images. The fracture size was normalized between 0 and 1, where a fracture size of 1 indicates a deep and large fracture, while a fracture size of close to 0 a

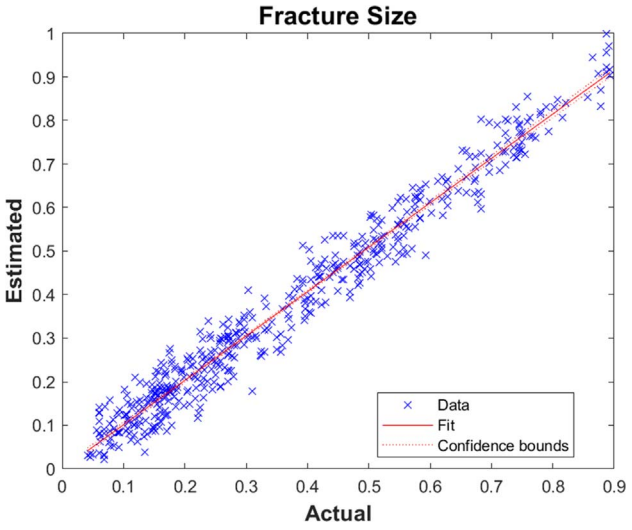

Figure 7. Comparison of estimated versus actual fracture sizes for the image deep learning framework for the testing set.

shallow and small fracture. A regression analysis (Fig. 7) outlines the estimates fracture size versus the actual size on the testing set. The performance of the framework is strong, enabling to accurately estimate fracture sizes and thereby determining potential dissipation of carbon dioxide into the reservoir. Confidence intervals are well within bounds of 0.05 that indicate high confidence in the estimates. The RMSE is 0.0449, with the coefficient of determination being 0.965. The ground truth was validated based on expert interpretation of the fracture images.

5 Conclusion

We have presented a new deep learning framework for the detection of fractures in formation image logs for enhancing CO_2 storage. Fractures may represent high velocity gas flow channels which may make CO_2 storage a challenge. The novel deep learning framework incorporates both acoustic and electrical formation image logs for the detection of fractures in wellbores for CO_2 storage enhancement and injection optimization. The framework was evaluated on the Pohokura-1 well for the detection of fractures, with the framework exhibiting strong classification accuracy.

References

Aghli G., Moussavi-Harami R., Mohammadian R. (2020) Reservoir heterogeneity and fracture parameter determination using electrical image logs and petrophysical data (a case study, carbonate Asmari Formation, Zagros Basin, SW Iran), *Pet. Sci.* **17**, 1, 51–69.

Andreasen A. (2021) Optimisation of carbon capture from flue gas from a Waste-to-Energy plant using surrogate modelling and global optimisation, *Oil Gas Sci. Technol. – Rev. IFP Energies nouvelles* **76**, 55.

Bihani A., Daigle H., Santos J.E., Landry C., Prodanović M., Milliken K. (2022) MudrockNet: Semantic segmentation of mudrock SEM images through deep learning, *Comput. Geosci.* **158**, 104952.

El Ouahed A., Tiab D., Mazouzi A. (2005) Application of artificial intelligence to characterize naturally fractured reservoirs, in: *Canadian International Petroleum Conference*, June 7–9, Calgary.

Fornero S.A., Marins G.M., Lobo J.T., Freire A.F.M., de Lima E.F. (2019) Characterization of subaerial volcanic facies using acoustic image logs: Lithofacies and log-facies of a lava-flow deposit in the Brazilian pre-salt, deepwater of Santos Basin, *Mar. Pet. Geol.* **99**, 156–174.

Ghiat I., Al-Ansari T. (2021) A review of carbon capture and utilisation as a CO_2 abatement opportunity within the EWF nexus, *J. CO_2 Util.* **45**, 101432.

Hassall J.K., Ferraris P., Al-Raisi M., Hurley N.F., Boyd A., Allen D.F. (2004) Comparison of permeability predictors from NMR, formation image and other logs in a carbonate reservoir, in: *Abdu Dhabi International Conference and Exhibition*, October 10–13, Abu Dhabi, United Arab Emirates.

Li T., Wang R., Wang Z., Zhao M., Li L. (2018) Prediction of fracture density using genetic algorithm support vector machine based on acoustic logging data, *Geophysics* **83**, 2, 49–60.

Rezig D. (2019) Fracture aperture estimation using electrical image logs (FMI) and acoustic (SS), in: *Fifth EAGE/AAPG Tight Reservoirs Workshop*, European Association of Geoscientists & Engineers, pp. 1–6.

Tian X., Daigle H. (2018) Machine-learning-based object detection in images for reservoir characterization: A case study of fracture detection in shales, *Lead. Edge* **37**, 6, 435–442.

Tursunov O., Kustov L., Kustov A. (2017) A brief review of carbon dioxide hydrogenation to methanol over copper and iron based catalysts, *Oil Gas Sci. Technol. – Rev IFP Energies nouvelles* **72**, 5, 9.

Valentín M.B., Bom C.R., Coelho J.M., Correia M.D., Márcio P., Marcelo P., Faria E.L. (2019) A deep residual convolutional neural network for automatic lithological facies identification in Brazilian pre-salt oilfield wellbore image logs, *J. Petrol. Sci. Eng.* **179**, 474–503.

Vidal J., Genter A., Schmittbuhl J. (2016) Pre-and post-stimulation characterization of geothermal well GRT-1, Rittershoffen, France: Insights from acoustic image logs of hard fractured rock, *Geophys. J. Int.* **206**, 2, 845–860.

Wang M., Fan Z., Zhao L., Xing G., Zhao W., Tan C. (2020) Productivity analysis for a horizontal well with multiple reorientation fractures in an anisotropic reservoir, *Oil Gas Sci. Technol. – Rev. IFP Energies nouvelles* **75**, 80, 17.